International Journal of Applied Sciences: Current and Future Research Trends (IJASCFRT)
ISSN: 2790-3990

https://ijascfrtjournal.isrra.org/index.php/Applied_Sciences_Journal

Analysis and Simulation of Horizontal Axis Wind Turbine Control Using Coefficient Diagram Method / Two-Mass Model

A. Mfedel[a*], A. Djebli[b]

[a,b]*Laboratory of energetic, Faculty of science, Abdelmalek Essadi University, BP. 2121 M'Hannech II, Tetouan, Morocco*

[a]*Email: akdi.m_ffedal-etu@uae.ac.ma*

[b]*Email: djebli_abdelouahed@yahoo.fr*

Abstract

In this paper, the Coefficient Diagram Method is used to control the two-mass drive train system. For this, a first-order plus time delay (FOPTD) model is used. The various approaches used in the FOPTD are analyzed, and the polynomial controller has been designed, and its control action is discussed. As a result, for the two-mass system, it is observed that the designed polynomial CDM controller exhibits better outcomes for the TD approximation followed by the Padé approximation. However, the TN approximation is generally not recommended for successful performance.

Keywords: Two-mass system; Coefficient Diagram Method; FOPDT.

I. Introduction

One of the furthermost widely used control laws is the PID type controller, With its three terms functionality covering dealing with both transient and steady states response, PID controller offers the simplest and efficient solution for different real control problems. In a two-mass resonant system, PID plays a principal role for the control of the system responses, and many other methods have been used for the system control such as resonance ratio approach, pole placement, and optimal control [1,2,3,4]. PID controller design aims to determine a set of gains in such a way to meet the transient response, the disturbance rejection, and the steady-state error. However, in various applications and practices, it is not possible to reach all of these objectives. A coefficient diagram method is a novel approach for design controllers. CDM control technique, introduced by Manabe in 1991 [1], is an algebraic method applied to the polynomial loop, where a coefficient diagram is used as a criterion for good design. The Coefficient Diagram Method (CDM) is an indirect pole placement method to design an appropriate characteristic polynomial [5].

---

* Corresponding author.

The transfer function is specified before the controller's design, and the performance specification is rewritten instability index and equivalent time constant. These parameters specify the closed-loop transfer function. Also, these parameters are related to the controller parameters algebraically in explicit form. This paper's main purpose is the application of the CDM method to proposal a controller for the plant such that the control system realizes the wanted performance. For this, a method for short time delays compensation based on approximations of the FOPTD [6] is presented. The three-time delay approximations are used and compared: Taylor denominator expansions, Taylor numerator, and Padé approximation. The paper is systematized as follows: Section 2 provides a modeling turbine of the variable speed wind turbine (VSWT). Section 3 provides a mathematical model of the Two-mass system structure. Section 4 describes the control objectives and the designs of the control system by CDM. After this, the basic control structure is determined using CDM, a feedback controller designed as a MISO problem, and derivation of the controller tuning formulae for the FOPTD plant model of the stable processes is given. The three-time delay approximations: Taylor denominator (TD) expansions, Taylor numerator (TN), and Padé approximation (PA). In section 5, the effectiveness and robustness of the proposed method are demonstrated by simulation results. In the finish, simulation results are shown for these controllers.

II. Modeling turbine physics

The power of an air mass that flows at speed V through an area A can be expressed as:

$$P_w = \frac{1}{2}\rho A V^3 \tag{1}$$

Where $\rho(\mathrm{kg/m^3})$ the Air density and $V(m/s)$ the Wind speed. The power in the wind is the total obtainable energy per unit of time. The wind's power is transformed into the mechanical–rotational energy of the wind turbine rotor, which results in a reduced speed in the air mass. The wind power cannot be extracted completely by a wind turbine, as the air mass would be stopped completely in the catching rotor area. This would cause a 'congestion' of the cross-sectional area for the following air masses.

The fraction of power (P_m) extracted from the available power in the wind (P_w) by practical turbines is expressed by the coefficient of performance, (C_p). The power extracted (P_m) can then be expressed as shown in equation (2).

$$P_m = \frac{1}{2}\rho A V^3 C_p(\lambda, \beta) \tag{2}$$

The value of $C_p(\lambda, \beta)$ varies with the wind speed, the turbine blade parameters' rotational speed, the rotor pitch angle, and the turbine blade parameters. According to Betz, the theoretical maximum power extracted

from the wind cannot exceed $C_{p_{Betz}} = 16/27$. The tip speed ratio is a variable that combines the effects of the rotational speed and the wind speed. It is defined as the ratio between the rectilinear speed of the turbine:

$$\lambda = \frac{\omega R}{V} \tag{3}$$

The wind turbine rotor performance can also be estimated as a function of the coefficient of torque C_q, where the torque T_a is:

$$T_a = \frac{P_m}{\omega} \tag{4}$$

C_q can be related to the power coefficient, C_p through the relation:

$$C_q(\lambda, \beta) = \frac{C_p(\lambda, \beta)}{\lambda} \tag{5}$$

and the aerodynamic torque T_a, can be expressed as:

$$T_a = \frac{1}{2}\rho A R V^2 C_q(\lambda, \beta) \tag{6}$$

Therefore, manipulation of the torque coefficient using λ and β will result in manipulate the power produced by the turbine.

For models C_p as a function of the tip speed ratio and the blade pitch angle β in degrees as:

$$C_p(\lambda, \beta) = 0.5\left(\frac{116}{\lambda_i} - 0.4\beta - 5\right) e^{\left(-\frac{21}{\lambda_i}\right)} + 0.0068\lambda \tag{7}$$

the parameter $\frac{1}{\lambda_i} = \frac{1}{\lambda - 0.08\beta} - \frac{0.035}{1+\beta^3}$ defined in [7].

The torque coefficient C_q of the wind turbine can be expressed as a function of the tip speed ratio λ and the blade pitch angle of the wind β in [8]. The Power coefficient C_p calculated for different tip speed ratios λ and different blade pitch angle β, is presented in Fig.1 and 2.

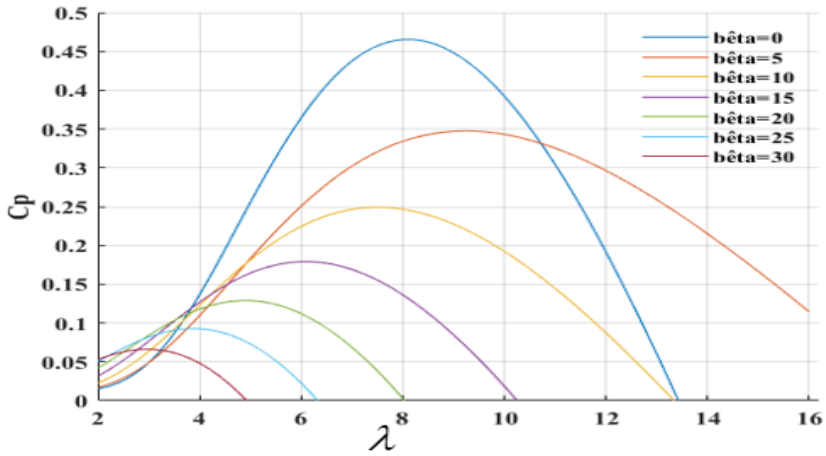

Figure 1: Analytical approximation of $C_p(\lambda,\beta)$ characteristics

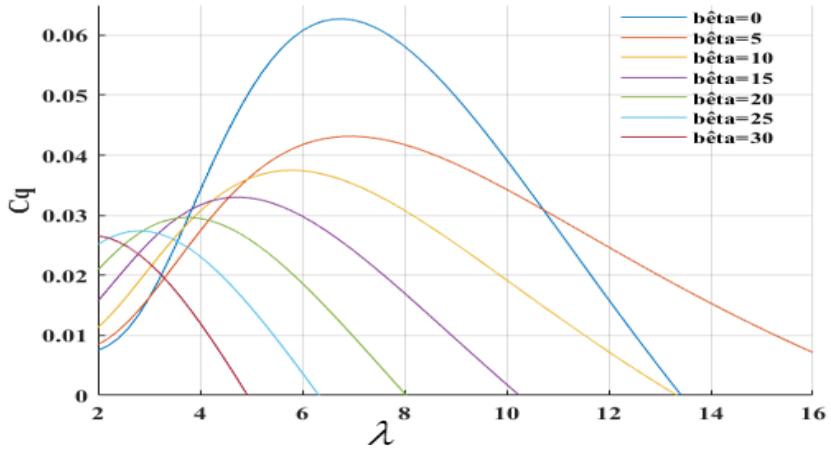

Figure 2: Analytical approximation of $C_q(\lambda,\beta)$ characteristics

The global maximum for the power coefficient is at null pitch angle and it is equal to:

$$C_{P_{\max}}(\lambda_{opt},\beta=0)=0.4654 \tag{8}$$

corresponding to an optimal tip speed ratio at null pitch angle equal to $\lambda_{opt}=8.2$,[9].

III. Two-mass model

The two-mass model representation of the drive system dynamics is shown in Fig.3.A wind turbine's mechanical rotational system generally comprises a rotor, low-speed shaft, gearbox, high-speed shaft, and generator rotor [10].

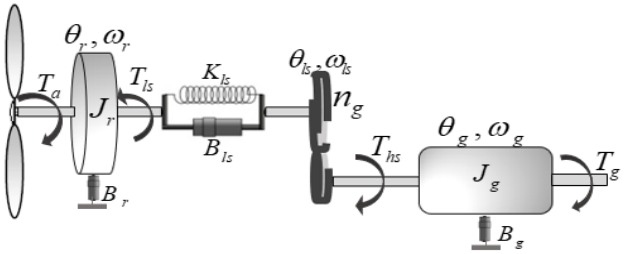

Figure 3: Two-mass wind turbine model

The nominal parameters for the two-mass model in this article are given in Table 1 below

Table1: Two-mass model Parameters[11]

Symbol	Quantity	Value
K_{ls}	Shaft stiffness coefficient	269100 Nm/rad
B_{ls}	Shaft damping coefficient	9500 Nm/rad/s
B_r	Rotor damping coefficient	27.36 Nm/rad/s
B_g	Generator damping coefficient	0.2 Nm/rad/s
J_r	Rotor inertia	325000 Kg. m^2
J_g	Generator inertia	34.4 Kg. m^2
n_g	Gearbox Ration	43.165

The state equation of two-mass resonant system is as follows [12]. The rotor inertia J_r is driven at a speed ω_r by the aerodynamic torque T_a. Its dynamics are described by:

$$\frac{d\omega_r}{dt} = \frac{T_a}{J_r} - \frac{T_{ls}}{J_r} - \frac{B_r}{J_r}\omega_r \tag{9}$$

The generator inertia J_g is driven by the high-speed shaft and braked by the electromagnetic torque T_g. Its dynamics are described by:

$$\frac{d\omega_g}{dt} = \frac{T_{hs}}{J_g} - \frac{T_g}{J_g} - \frac{B_g}{J_g}\omega_g \tag{10}$$

Where, B_r is the rotor viscous damping coefficient, and B_g is the generator viscous damping coefficient. The low-speed shaft torque T_{ls} acts as a braking torque on the rotor. Indeed, it results from stiffness K_{ls} and damping B_{ls} efforts due to the difference between ω_r and ω_{ls} is given by[13]:

$$T_{ls} = K_{ls}(\theta_r - \theta_{ls}) + B_{ls}(\omega_r - \omega_{ls}) \tag{11}$$

The torque and the speed of this shaft are transmitted via the gearbox with a rate ratio n_g . For an ideal gearbox, one has:

$$n_g = \frac{T_{ls}}{T_{hs}} = \frac{\omega_g}{\omega_{ls}} = \frac{\theta_g}{\theta_{ls}} \tag{12}$$

From (11) to (12):

$$\frac{dT_{ls}}{dt} = (K_{ls} - \frac{B_{ls}B_r}{J_r})\omega_r - B_{ls}(\frac{J_r + J_g n_n^2}{J_r J_g n_g^2})T_{ls} - \frac{1}{n_g}(\mathrm{K}_{ls} - \frac{B_{ls}B_g}{J_g})\omega_g + \frac{B_{ls}}{J_r}T_a + \frac{B_{ls}}{J_g n_g}T_g \tag{13}$$

The linear drive train model developed from (10-13) can be expressed in the state space form as [14]:

$$\begin{cases} \dot{X} = AX + BU \\ Y = CX \end{cases} \tag{14}$$

$$A = \begin{bmatrix} -\frac{B_r}{J_r} & -\frac{1}{J_r} & 0 \\ K_{ls} - \frac{B_{ls}B_r}{J_r} & -B_{ls}(\frac{J_r + J_g n_g^2}{J_r J_g n_g^2}) & -\frac{1}{n_g}(K_{ls} - \frac{B_{ls}B_g}{J_g}) \\ 0 & \frac{1}{J_g n_g} & -\frac{B_g}{J_g} \end{bmatrix}, \quad B = \begin{bmatrix} \frac{1}{J_r} & 0 & 0 \\ \frac{B_{ls}}{J_r} & 0 & \frac{B_{ls}}{J_g n_g} \\ 0 & 0 & -\frac{1}{J_g} \end{bmatrix} \tag{15}$$

$$C = I_{(3,3)}\ , \quad U = \begin{bmatrix} T_a & 0 & T_g \end{bmatrix}^T \quad \text{and} \quad X = \begin{bmatrix} \omega_r & T_{ls} & \omega_g \end{bmatrix}^T \tag{16}$$

and the block diagram representation of the two-mass system is shows in Fig.4. Let a two-input and three-output process be represented by the block diagram shown in Fig.5 for which the transfer function [14]is:

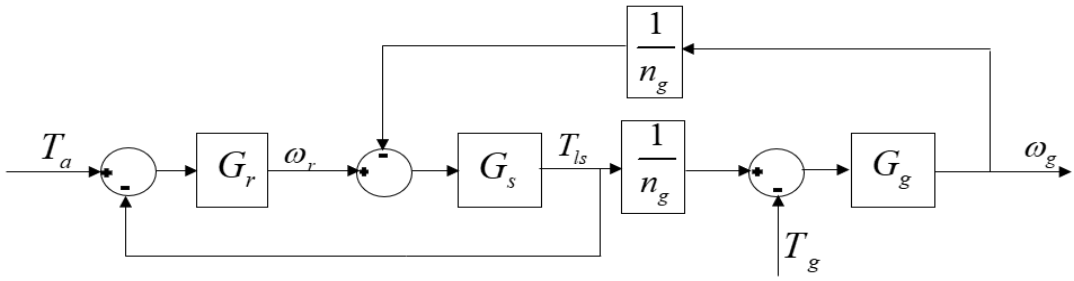

Figure 4: Block diagram of the two-mass mechanical system

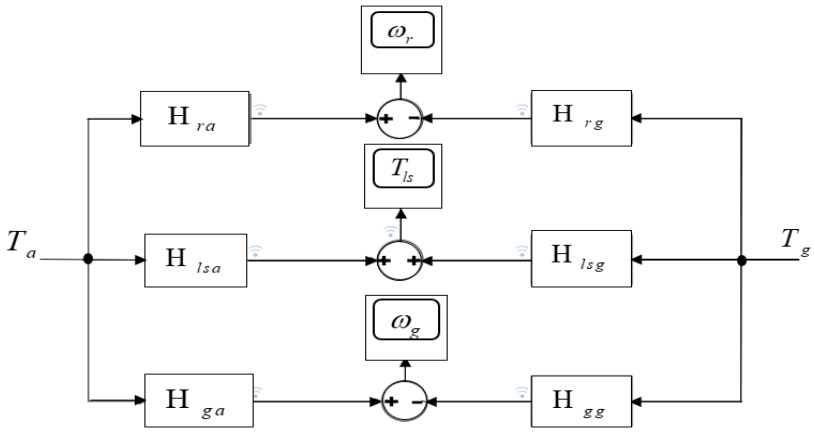

Figure 5: Two-input and three-output of the system

where:

$$\begin{bmatrix} \omega_r(s) \\ T_{ls}(s) \\ \omega_g(s) \end{bmatrix} = \begin{bmatrix} H_{ra}(s) & -H_{rg}(s) \\ H_{lsa}(s) & H_{lsg}(s) \\ H_{ga}(s) & -H_{gg}(s) \end{bmatrix} \begin{bmatrix} T_a(s) \\ T_g(s) \end{bmatrix} \tag{17}$$

The rotor speed, shaft torque and generator speed are:

$$\omega_r = \frac{G_r(n_g^2 + G_s G_g)}{n_g^2 + n_g^2 G_s G_r + G_s G_g} T_a - \frac{n_g G_s G_g G_r}{n_g^2 + n_g^2 G_s G_r + G_s G_g} T_g \tag{18}$$

$$T_{ls} = \frac{n_g^2 G_r G_s}{n_g^2 + n_g^2 G_s G_r + G_s G_g} T_a + \frac{n_g G_s G_g}{n_g^2 + n_g^2 G_s G_r + G_s G_g} T_g \tag{19}$$

$$\omega_g = \frac{n_g G_s G_g G_r}{n_g^2 + n_g^2 G_s G_r + G_s G_g} T_a - \frac{G_g n_g^2 (1 + G_s G_r)}{n_g^2 + n_g^2 G_s G_r + G_s G_g} T_g \tag{20}$$

Transfer functions of the rotor, shaft and generator are:

$$G_r = 1/J_r s + B_r, \quad G_s = B_{ls} s + K_{ls}/s, \quad G_g = 1/J_g s + B_g \tag{21}$$

Using:

$$H_{ra}(s) = \left.\frac{\omega_r(s)}{T_a(s)}\right|_{T_g=0} = \frac{1}{n_g^2 J_g J_r} \frac{n_g^2 J_g s^2 + (n_g^2 B_g + B_{ls})s + K_{ls}}{\Delta(s)} \tag{22}$$

$$H_{lsa}(s) = \left.\frac{T_{ls}(s)}{T_a(s)}\right|_{T_g=0} = \frac{1}{n_g^2 J_g J_r} \frac{(B_{ls}s + K_{ls})(J_g s + B_g)}{\Delta(s)} \tag{23}$$

$$H_{ga}(s) = \left.\frac{\omega_g(s)}{T_a(s)}\right|_{T_g=0} = \frac{1}{n_g^2 J_g J_r} \frac{n_g (B_{ls}s + K_{ls})}{\Delta(s)} \tag{24}$$

where the characteristic equation of the open loop system is given as:

$$\Delta(s) = s^3 + \left(\frac{B_r + B_{ls}}{J_r} + \frac{n_g^2 B_g + B_{ls}}{n_g^2 J_g}\right)s^2 + \left(\frac{K_{ls}(n_g^2 J_g + J_r) + B_{ls}(n_g^2 B_g + B_r) + n_g^2 B_r B_g}{n_g^2 J_g J_r}\right)s + \frac{K_{ls}(n_g^2 B_g + B_r)}{n_g^2 J_g J_r} \tag{25}$$

Since their effect on resonance is negligible $B_r = 0$ and $B_g = 0$; so that, the resonance frequency ω_R, anti-resonance frequency ω_A, and the damping ratio ξ of the drive chain are [5]:

$$\omega_R = \sqrt{K_{ls}\left(\frac{1}{J_r} + \frac{1}{J_g n_g^2}\right)}, \quad \omega_A = \sqrt{\frac{K_{ls}}{J_g n_g^2}}, \quad \xi = \frac{B_{ls}}{2\sqrt{K_{ls}}}\sqrt{\frac{1}{J_r} + \frac{1}{J_g n_g^2}} \tag{26}$$

The dominant eigenvalues for the open-loop system are $P_1 = -0.005814$ and $P_{2,3} = -0.0912 \pm 2.24$, The resonant frequency is $\omega_R = 2.242 rad/s$ and the anti-resonant frequency is $\omega_A = 2.05 rad/s$, The damping ratio of the drive chain is $\xi = 0.0396$. It can be seen that the system is stable, then all of the eigenvalues have negative real parts. The response frequency of transfer functions relative to rotor torque is shown in Fig.6. [5]:

Displays the frequency response characteristics of the two-mass resonance model from the rotor speed, shaft torque and generator speed. The peak point of the mechanical resonance can be perceived in this figure. It is therefore essential to concept the controller design method such that it reduces this resonance peak gain.

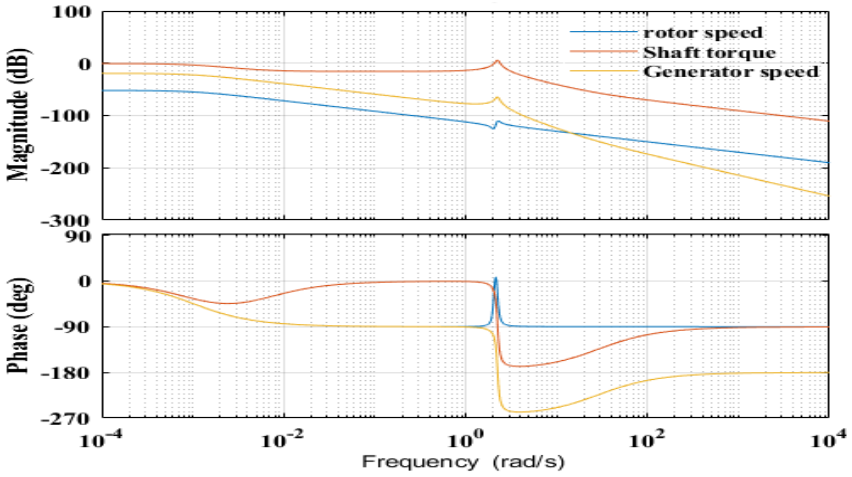

Figure 6: The response frequency of transfer function relative to aerodynamic torque rotor

IV. CDM Design Procedure

The concept of CDM was first proposed by Manabe (1991). The Coefficient Diagram Method (CDM) is an indirect pole placement method to design an appropriate characteristic polynomial [5]. It is very easy to strategy a controller under the conditions of stability, time-domain performance, and robustness. The basic block diagram of the CDM control system is shown in Fig.7a. In this figure, y is the output, r is the reference input signal, u is the control signal, and d is the external disturbance signal. The transfer function of the plant $G(s) = N(s)D^{-1}(s)$ where $N(s)$ and $D(s)$ are the numerator and the denominator of the $G(s)$, respectively $A(s)$, $B(s)$, and $F(s)$ are the polynomials syndicated with the CDM controller.

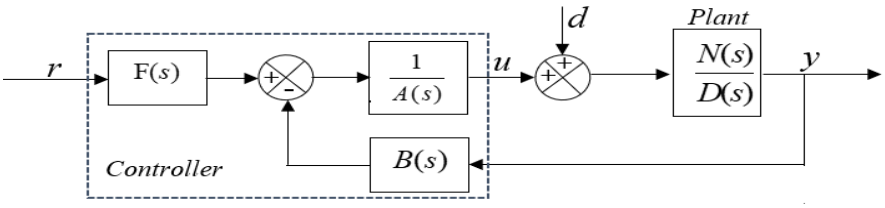

Figure 7a: A block diagram of CDM control system

The output of the controlled system is given by:

$$\mathrm{P}(s)\, y = N(s)F(s)\mathrm{r} + A(s)N(s)d \tag{27}$$

Where the characteristic polynomial $P(s)$ is given as the following form [1].

$$P(s) = A(s)D(s) + B(s)N(s) \tag{28}$$

Approximately mathematical relations extensively used in CDM will be introduced henceforth. These relations will be used in later section. In CDM, the transient response performance specifications were specified by means of two parameters such as γ_i and τ. These parameters were used to specify the closed loop transfer function. As will be explained later, stabi1ity index γ_i, equivalent time constant τ and stability limit indices γ_i^* are given by[15]:

$$\gamma_i = a_i^2 / a_{i+1} a_{i-1}, \qquad i = 1...n-1 \tag{29}$$

$$\tau = a_1 / a_0 \tag{30}$$

$$\gamma_i^* = 1/\gamma_{i-1} + 1/\gamma_{i+1}, \quad i = 1...n-1, \quad \text{where } \gamma_n = \infty \text{ and } \gamma_0 = \infty \tag{31}$$

From Eq.29-31, the coefficients a_i can be written as:

$$a_i = \frac{\tau^i}{\prod_{j=1}^{i-1} \gamma_{i-j}^j} a_0 = Z_i a_0 \quad \text{where } \mathrm{P}(s) = \sum_{i=0}^{n} a_i s^i \tag{32}$$

Using the relations in Equation (29,30, and 31), it is possible to formulate the characteristic polynomial $P_{target}(s)$ in terms of the design parameters τ and γ_i as follows:

$$P(s) = a_0 \left[\left\{ \sum_{i=2}^{n} \left(\prod_{J-1}^{i-1} \frac{1}{\gamma_{i-j}^j} \right) (\tau s)^i \right\} + \tau s + 1 \right] \tag{33}$$

where: $P_{target}(s)$ - is the Target Characteristic Polynomial.

Now, the problem is here how to select the appropriate controller parameters in terms of stability, minimum overshoot and robustness. Manabe proposed that γ_1 should equal to 2.5, γ_2, and γ_3 should be equal to 2 to ensure the stability of fourth-order closed-loop systems [16].

V. CDM Control structure

CDM used a simultaneous approach to obtain the controller and closed-loop transfer function, and it uses to design a simple polynomial controller for stable first Order Plus Time Delay (FOPTD) systems with an external disturbance. In this paper, the process to be controlled is represented or assumed to be approximated as a FOPTD model whose transfer function is given by:

$$G(s) = \frac{K}{1+Ts}\exp(-Ls) \tag{34}$$

Where:

K – Gain coefficient: the ultimate value of the response (new steady state) for a unit step change in the input.

T – Time constant: measure of time wanted for the process to adjust to a change in the input

L – Delay: the time at which output of the system starts to change minus the time at which the input step change was made [17].

Approximate a high order open loop system using FOPDT. If the system model cannot be physically derived, experiments can be performed to extract the parameters for the approximate model (34). For instance, if the step response of the plant model can be measured through an experiment, from which the parameters of k, L, and T can be extracted by the simple approach shown[18]. The CDM control system was designed by approximating the time delay using Taylor Numerator (TN) expansion, Taylor Denominator (TD) expansion, and Pade Approximation (PA) techniques. The experimental identification of this model using many techniques is well described in [19]. The term e^{-Ls} which represents the time delay in Eq.34 is approximated by:

- The Taylor numerator expansion: $e^{-Ls} \approx 1 - Ls$ (35)
- The Taylor denominator expansion: $e^{-Ls} \approx \frac{1}{1+Ls}$ (36)
- The Padé approximation: $e^{-Ls} \approx \frac{2-Ls}{2+Ls}$ (37)

These approximations can positively be used for the time delay if the ratio of the time delay to the time constant is small. The first order approximations are sufficient because their higher number leads to a higher order of a controlled system's approximative transfer function and, consequently, to more complex resulting controllers. The equivalent linear time-invariant models of Eq.34 are obtained as in Table.2.

V.1 Determination of the nominal plant and the controller polynomials

Fig.7b represents the standard block diagram of the control system designed by CDM. It is composed of a plant and CDM controller. The transfer function of the plant is thought to be two independent polynomials, one is the numerator polynomial $N(s)$ of degree m, and the other is the denominator polynomial $D(s)$ of degree n(m<n).

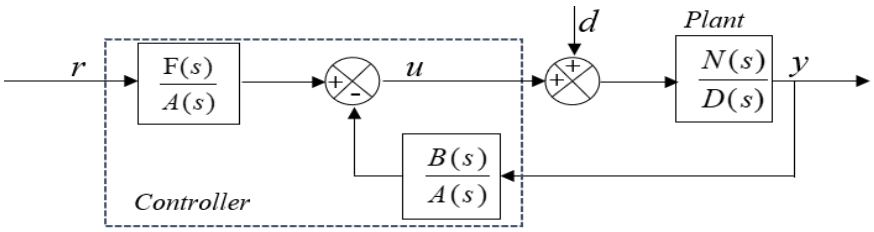

Figure 7b: Simulation block diagram for the CDM control system

The polynomials $A(s)$, $B(s)$ are given by:

$$A(s)=\sum_{i}^{p} l_i s^i, \qquad B(s)=\sum_{i=0}^{q} k_i s^i \tag{38}$$

where the condition $p \geq q$ must be satisfied for practical realization. In this paper, the controller

Table2: Equivalent transfer Functions for Eq. 34

	Equivalent transfer Functions of FOPTD model
TN exp.	$G_{sn}=\frac{-KLs+K}{Ts+1}$
TD exp.	$G_{sd}=\frac{K}{TLs^2+(\mathrm{L}+\mathrm{T})\mathrm{s}+1}$
Padé	$G_{sp}=\frac{-KLs+2K}{TLs^2+(\mathrm{L}+2\mathrm{T})\mathrm{s}+2}$

polynomials are chosen for the step disturbance signal. The controller polynomials then have forms:

$$A(s)=l_1 s \tag{39a}$$

$$B(s)=K_1 s+K_0 \tag{39b}$$

for the numerator approximation and;

$$A(s)=l_2 s^2+l_1 s \tag{40a}$$

$$B(s)=K_2 s^2+K_1 s+K_0 \tag{40b}$$

For the denominator and Padé approximations.

V.2 Computation of the coefficients of the controller polynomials during the design

The pole-placement method is made use of in the calculation of the controller polynomials in CDM. A feedback controller is selected by pole placement technique, and then, a feedforward controller is determined to match the steady-state gain of a closed-loop system. According to this, the controller polynomials which are determined by Eq. 39 and 40 are replaced in Eq. 28. This way a polynomial depending on the parameters k_i and l_i are obtained. Then, a target characteristic polynomial $P_{target}(s)$ is determined by placing the design parameters into Eq. 33. Equating these two polynomials,

$$P_{target}(s) = A(s)D(s) + B(s)N(s) = \sum_{i=0}^{n} a_i s^i \qquad (41)$$

which is known to be a Diophantine equation. Solving this equation, the following explicit formulae are found for the coefficients of the controller polynomials $A(s)$ and $B(s)$ in Eq. 39 and 40.

The parameters of Eqs. 39a and 40b can be described as:

Table3: coefficients of the controller polynomials $\mathrm{A}(s)$ and $\mathrm{B}(s)$

Coefficients of the control polynomials A(s) and B(s)	For the numerator approximation	For the denominator approximation	For the padé approximation
K_0	$\frac{1}{K}$	$\frac{1}{K}$	$\frac{0.5}{K}$
K_1	$\frac{\tau + L - l_1}{K}$	$\frac{\tau - l_1}{K}$	$\frac{\tau + 0.5L - 2l_1}{K}$
K_2		$\frac{Z_2 - (T+L)l_1 - l_2}{K}$	$\frac{TLl_1 - 2(T+L)l_2 - Z_4}{KL}$
l_1	$\frac{Z_2\tau^2 + L\tau + L^2}{T+L}$	$\frac{Z_3 - (T+L)l_2}{TL}$	$\frac{L^3 + 2L^2\tau + 4L(Z_2 - 4l_2) + 8(Z_3 - 2Tl_2)}{8L(2T+L)}$
l_2		$\frac{Z_4}{LT}$	$\frac{Z_4}{LT}$
$F(s)\|_{s=0}$	$\frac{1}{K}$	$\frac{1}{K}$	$\frac{0.5}{K}$

F(s) which is commonly defined as pre-filter element is chosen as:

$$F(s) = P(s)/N(s)\big|_{s=0} = P(0)/N(0) \qquad (42)$$

This way, the steady-state error in the closed loop system performance is reduced to zero.

VI. controller applied

design considerations of the proposed Controller by the Coefficient Diagram Method are given, Fig.8, 9 and 10 show a close-loop with $G_f(s) = F(s)/B(s)$ and $G_v(s) = B(s)/A(s)$ controllers. The block diagram of rotor speed, shaft torque and generator speed are represented as:

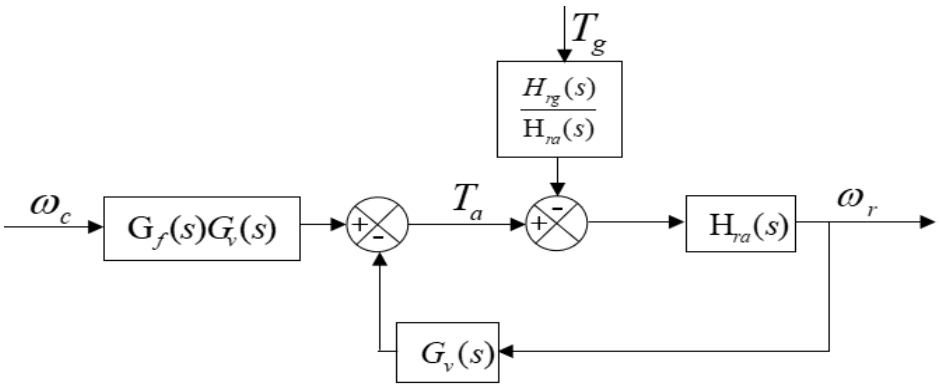

Figure 8: Block diagram of rotor speed system with $G_f(s)$ and $G_v(s)$ controllers

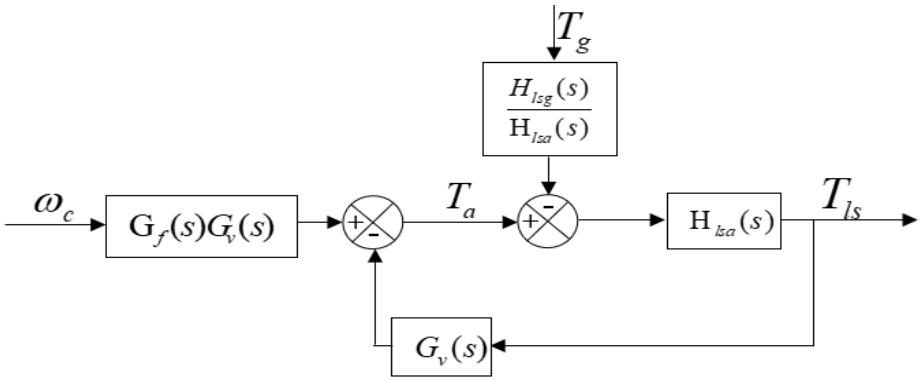

Figure 9: Block diagram of shaft torque system with $G_f(s)$ and $G_v(s)$ controllers

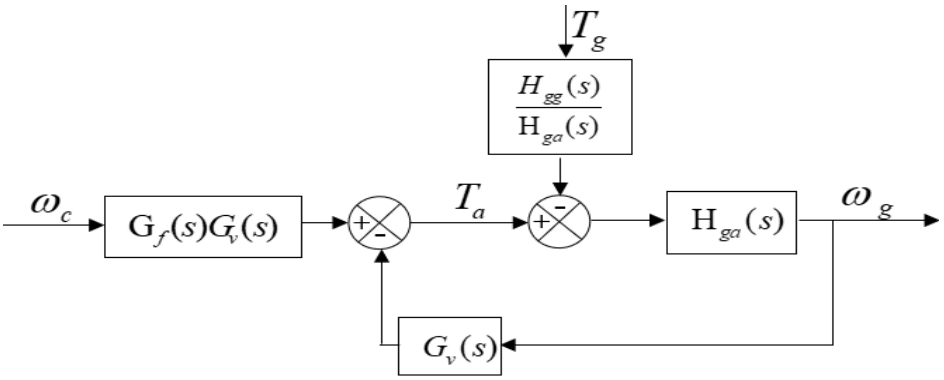

Figure 10: Block diagram of generator speed system with $G_f(s)$ and $G_v(s)$ controllers

The closed-loop transfer function from the command ω_C to the rotor speed, the shaft torque and the generator speed are [20]:

$$\left.\frac{\omega_r(s)}{\omega_C(s)}\right|_{T_g=0} = \frac{G_v(s)G_f(s)H_{ra}(s)}{1+G_v(s)H_{ra}(s)} \tag{43}$$

$$\left.\frac{T_{ls}(s)}{\omega_C(s)}\right|_{T_g=0} = \frac{G_f(s)G_v(s)H_{lsa}(s)}{1+G_v(s)H_{lsa}(s)} \tag{44}$$

$$\left.\frac{\omega_g(s)}{\omega_C(s)}\right|_{T_g=0} = \frac{G_f(s)G_v(s)H_{ga}(s)}{1+G_v(s)H_{ga}(s)} \tag{45}$$

The characteristic equation of Closed loop system is obtained by using the following expression:

$$N(s) = G_r(n_g^2 + G_s(s)G_g(s)) \tag{46}$$

$$D(s) = n_g^2 + n_g^2 G_s(s)G_r(s) + G_s(s)G_g(s) \tag{47}$$

VII. Simulation results

In this unit, we verify the validity of the proposed method. MATLAB executes all simulations. A two-mass wind turbine model is given to illustrate the CDM's performance in the design of a simple controller for a time-delay system. The CDM control system is designed using three approximations for the various ratio between the time delay and the time constant of the FOPTD system.The open-loop step response is shown in Fig.11. The graph shows three parameters, L the delay time, T the time constant and K the gain. These parameters are found by drawing a tangent to the step response at its point of inflection, followed by noticing its intersections with the time axis and the stable state value. From this step response, the parameters of the approximate FOPDT model for rotor speed are k = 0.0025, L = 0.1, and T = 1000s.

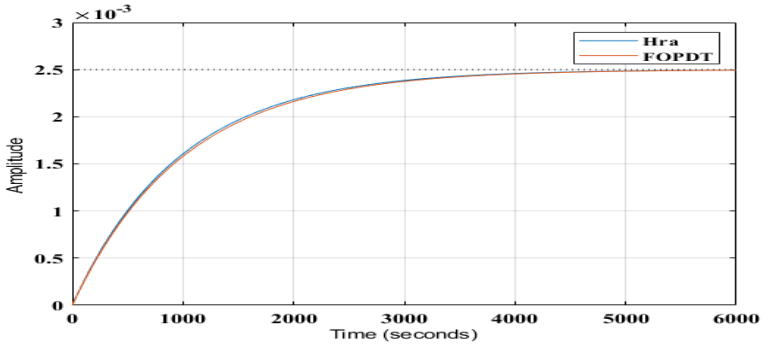

Figure 11: open-loop step response of rotor speed for the approximate FOPDT

In this section, rotor speed, shaft torque and generator speed are given in order to illustrate the performance of the CDM in the design of simple controllers for time-delay systems. The CDM control systems are delineated

using three approximations for the various ratio between the time delay and the time constant of the FOPTD system. The effect of stability indices and equivalent time constant on the system performance is investigated (Fig.12, 14, 16).

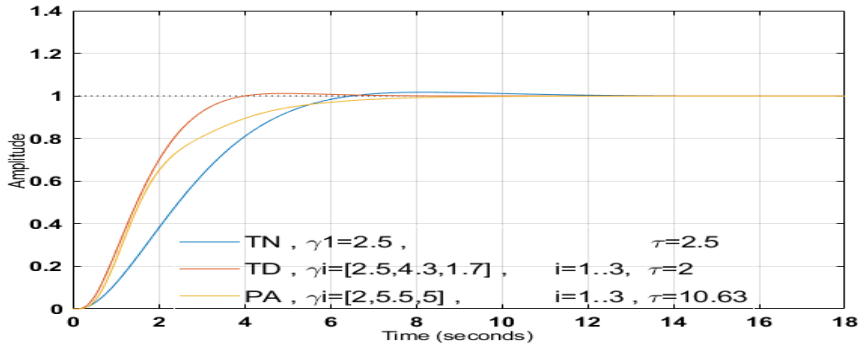

Figure 12: Step response of rotor speed for the TN, TD, and PAD approximations

The unit step response of the wind turbine the rotor speed control system is shown in Fig 12. Time-domain specifications are observed from the response graphs and tabulated in Table 4. We observed less rise time and less settling time with TD approximation than TN and Padé approximations and a no overshoot.

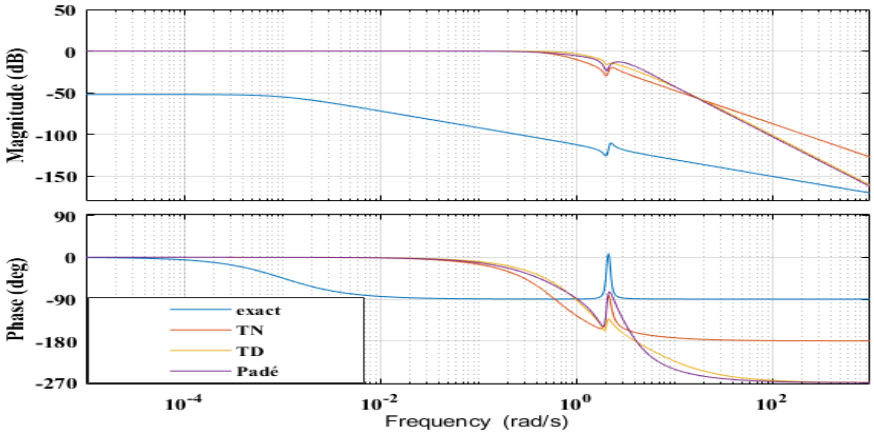

Figure 13: Amplitude and phase responses of $H_{ra}(s)$ and the TN, TD, and PAD approximations

The rotor speed $H_{ra}(s)$ is illustrated in Fig.13. The presented method's effectiveness is assured by the characteristic shown in this figure because the resonance peak is reduced considerably.

Table 4: Comparison between TN, TD and Padé

Time Domain	Without controller	TN exp	TD exp	Padé
Settling Time (sec)	3.8053e+03	8.4177	4.4453	6.3201
Rise Time (sec)	2.1373e+03	4.5846	2.4800	3.9824
Overshoot (%)	0	0	0	0

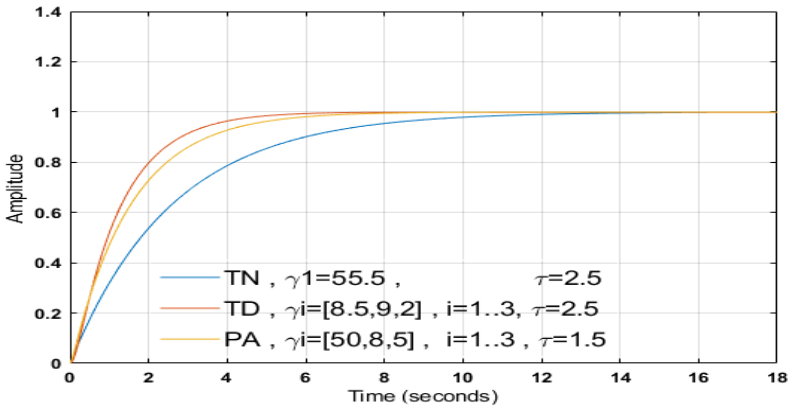

Figure 14: Step response of shaft torque for the TN, TD, and PAD approximations

The unit step response of the wind turbine the shaft torque control system is shown in Fig.14. Time-domain specifications are observed from the response graphs and tabulated in Table.5. We observed less rise time and less settling time with TD approximation than TN and Padé approximations and a no overshoot.

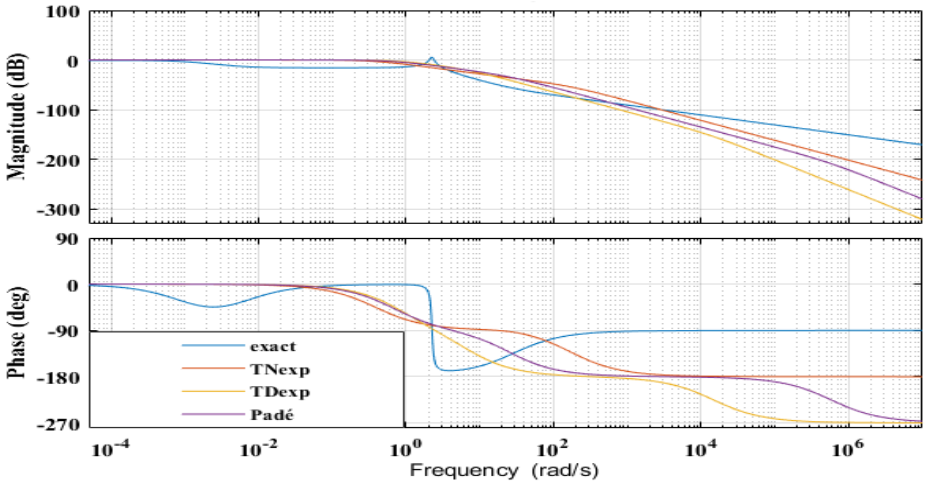

Figure 15: Amplitude and phase responses of $H_{lsa}(s)$ and the TN, TD, and PAD approximations

The shaft torque $H_{lsa}(s)$ is illustrated in Fig.15. The presented method's effectiveness is assured by the characteristic shown in this figure because the resonance peak is reduced considerably.

Table 5: Comparison between TN, TD and Padé

Time Domain	Without controller	TN exp	TD exp	Padé
Settling Time (sec)	3.6161e+03	9.7254	4.5911	5.8228
Rise Time (sec)	2.0500e+03	5.3920	2.5151	3.2285
Overshoot (%)	0	0	0	0

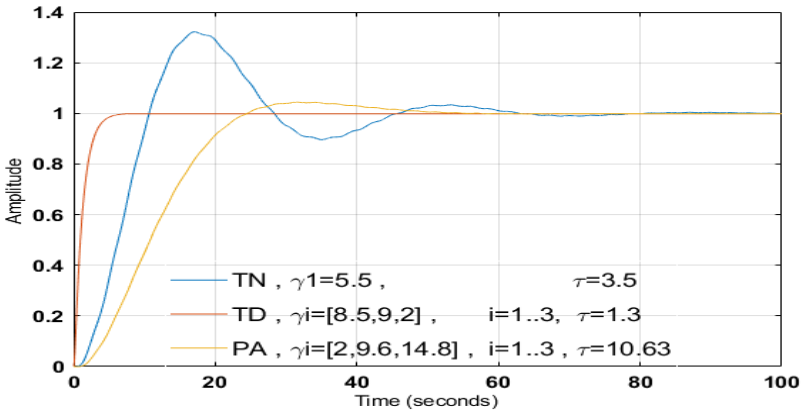

Figure 16: Step response of Generator speed the TN, TD, and PAD approximations

The unit step response of the wind turbine the generator speed control system is shown in Fig.16. Time-domain specifications are observed from the response graphs and tabulated in Table.6. We observed less rise time and less settling time with TD approximation than TN and Padé approximations and a very little overshoot.

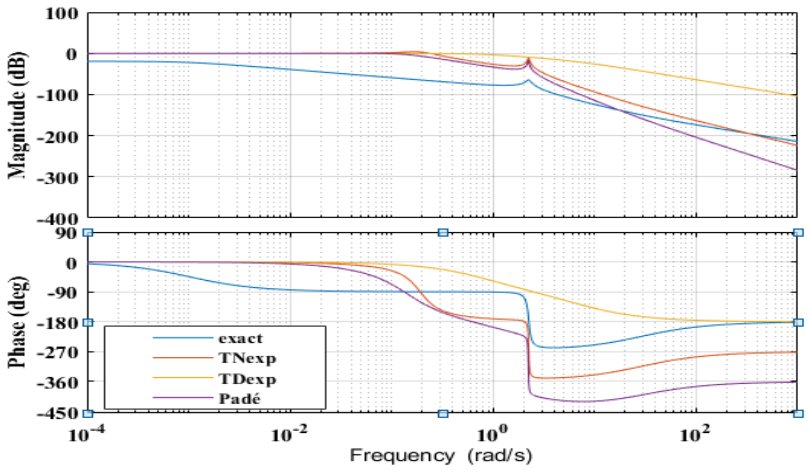

Figure 17: Amplitude and phase responses of $H_{ga}(s)$ and the TN, TD, and PAD approximations

The generator speed $H_{ga}(s)$ is illustrated in Fig.17. The presented method's effectiveness is assured by the characteristic shown in this figure because the resonance peak is reduced considerably.

Table 6: Comparison between TN, TD and Padé

Time Domain	Without controller	TN exp	TD exp	Padé
Settling Time (sec)	3.8053e+03	58.0168	4.5911	42.9715
Rise Time (sec)	2.1373e+03	7.1707	2.5151	15.2644
Overshoot (%)	0	32.6847	0	4.3489

VIII. Conclusion

The coefficient diagram method design technique used to design a two-mass model wind turbine controller gives very stable and robust control systems, small overshoot system responses, short stabilization time, and good robustness performance about mismatches between the actual system and the design model. As a result, for the two-mass system, it is observed that the designed polynomial CDM controller exhibits better results for the TD approximation followed by the Padé approximation. However, the TN approximation is generally not recommended for successful performance.

References

[1] R. Hirokawa and K. Sato, "Autopilot Design for a Missile with Reaction-Jet Using Coefficient Diagram Method," no. August, pp. 1–8, 2001.

[2] I. Kaya, N. Tan, and D. P. Atherton, "A simple procedure for improving performance of PID controllers," *IEEE Conf. Control Appl. - Proc.*, vol. 2, pp. 882–885, 2003, doi: 10.1109/cca.2003.1223126.

[3] D. Chen and D. E. Seborg, "PI/PID controller design based on direct synthesis and disturbance rejection," *Ind. Eng. Chem. Res.*, vol. 41, no. 19, pp. 4807–4822, 2002, doi: 10.1021/ie010756m.

[4] U. Tochukwu, "Effects of PID Controller on a Closed Loop Feedback System EFFECTS OF A PID CONTROLLER IN CLOSED LOOP," *Res. Gate*, no. December, 2014, doi: 10.13140/2.1.2650.0167.

[5] G. Shahgholian, "Controller Design for Three-Mass Resonant System Based on Polynomial Method," *Int. J. Sci. Technol. Soc.*, vol. 5, no. 2, p. 13, 2017, doi: 10.11648/j.ijsts.20170502.11.

[6] J. Cvejn, "PI/PID controller design for FOPDT plants based on the modulus optimum criterion," *Proc. 2011 12th Int. Carpathian Control Conf. ICCC'2011*, pp. 60–65, 2011, doi: 10.1109/CarpathianCC.2011.5945816.

[7] B. S. Mózo, *济無No Title No Title*, vol. 53, no. 9. 2017.

[8] G. Azevedo, "Modeling of a Variable Speed Wind Turbine with a Permanent Magnet Synchronous Generator," no. ISlE, pp. 734–739, 2009.

[9] R. Melício, V. M. F. Mendes, and J. P. S. Catalão, "Wind turbines equipped with fractional-order controllers : Stress on the mechanical drive train due," no. May 2010, pp. 13–25, 2011, doi: 10.1002/we.

[10] M. Tahiri, A. Djebli, and A. Mimet, "Drivetrain flexibility effect on control performance of a horizontal axis wind turbine," *Int. J. Appl. Eng. Res.*, vol. 12, no. 16, pp. 5511–5519, 2017.

[11] B. Boukhezzar and H. Siguerdidjane, “Nonlinear control of variable speed wind turbines without wind speed measurement,” *Proc. 44th IEEE Conf. Decis. Control. Eur. Control Conf. CDC-ECC ’05*, vol. 2005, no. 3, pp. 3456–3461, 2005, doi: 10.1109/CDC.2005.1582697.

[12] B. A. F, “INNM % C ; = 7 7CBHFC @ GHF5H9 ; M : CF HF57 ? = B ; H < 9 A5L = AIA DCK9F DC = BH,” vol. 19, pp. 599–606, 2015, doi: 10.1016/j.protcy.2015.02.085.

[13] T. M. O’Sullivan, C. M. Bingham, and N. Schofield, “High-performance control of dual-inertia servo-drive systems using low-cost integrated SAW torque transducers,” *IEEE Trans. Ind. Electron.*, vol. 53, no. 4, pp. 1226–1237, 2006, doi: 10.1109/TIE.2006.878311.

[14] G. Shahgholian, J. Faiz, and P. Shafaghi, “Analysis and simulation of speed control for two-mass resonant system,” *2009 Int. Conf. Comput. Electr. Eng. ICCEE 2009*, vol. 2, no. August, pp. 666–670, 2009, doi: 10.1109/ICCEE.2009.41.

[15] S. E. Hamamci, “Simple Polynomial Controller Design by the Coefficient Diagram Method,” no. January 2004, 2014.

[16] S. Manabe, *COEFFICIENT DIAGRAM METHOD IN MIMO APPLICATION: AN AEROSPACE CASE STUDY*, vol. 38, no. 1. IFAC, 2005.

[17] R. Bakerey, K. Elssadig, D. Eltahir, and M. Hussien, “Function using FOPDT, SOPDT and SKOGESTAD in Control System,” *Int. J. Eng. Appl. Manag. Sci. Paradig.*, vol. 42, no. 01, p. 1, 2016.

[18] A. Patra, “PID Controller Tuning using Ziegler-Nichols Method for Speed Control of DC PID Controller Tuning using Ziegler-Nichols Method for Speed Control of DC Motor,” no. September, 2018.

[19] D. Xue, Y. Chen, D. P. Atherton, and G. Gu, “Linear Feedback Control—Analysis and Design with Matlab,” *IEEE Control Syst.*, vol. 29, no. 1, pp. 128–129, 2009, doi: 10.1109/MCS.2008.930839.

[20] J. P. Coelho, T. M. Pinho, and J. Boaventura-cunha, “Controller System Design Using the Coefficient Diagram Method,” 2016, doi: 10.1007/s13369-016-2235-y.